HiSST: 3rd International Conference on
High-Speed Vehicle Science Technology
14 -19 April 2024, Busan, Korea

Modellings of steady shock reflection with chemical heat release and the transition criteria between regular and Mach reflections

Haoyang LI[1], Zijian ZHANG[2], and Chun WANG[3]

Abstract

This paper presents a pioneering shock-detonation reflection theory and solves the transition criteria to provide a valuable reference for future oblique detonation engine (ODE) design. Initially, we investigate the structure of the oblique detonation wave (ODW) when the deflection angle θ is less than θ_{CJ}. We note that the numerical results differ from the theoretical solution predicted by weak underdriven (WU) ODW. When $\theta < \theta_{CJ}$, a Chapman-Jouguet (CJ) ODW followed by a Prandtl-Meyer isentropic expansion (P-M IE) wave is obtained. In light of this finding, we introduce a CJ + P-M IE theory to reconstruct the relationship between pressure p and θ for the segment of WU detonation polar. Together with the segment of overdriven detonation polar, a whole detonation polar is established. Then, we provide a shock-detonation reflection theory combining the traditional shock polar and the new detonation polar. By analyzing the steady regular reflection (RR) and Mach reflection (MR) structures, we found that the key flow field characteristics, such as the angle of the slip line and reflected ODW, corroborate well with the theory. This verifies the accuracy of shock-detonation reflection theory. Subsequently, we solve the detachment criterion and von Neumann (VN) criterion according to the shock-detonation reflection theory. There are two crucial threshold values: critical heat release Q_C and critical Mach number M_C. When $Q < Q_C$, the section of the WU ODW is not employed in the reflection theory. When $M < M_C$, the solution of the VN criterion will be absent. Finally, the transition criteria are verified by numerical simulation under two different heat release Q. The numerical detachment and VN angles are coincident with the theoretical ones. The computations can confirm that the shock-detonation reflection theory and transition criteria are correct in our study.

Keywords: *Wave reflection, Prandtl-Meyer expansion wave, Transition criteria, Numerical simulation*

1. Introduction

Detonation is an extreme combustion mode that is triggered by a strong leading shock wave, and it exhibits a high thermal cycle efficiency. An oblique detonation wave (ODW) is one type of detonations that is generated when a supersonic combustible mixture passes through a wedge-shaped obstacle. Applying the ODW, an advanced hypersonic air-breathing propulsion system concept, oblique detonation engine (ODE) [1], was proposed and is expected to have a simpler geometry, a shorter combustor, and better thrust performance than traditional scramjet engines.

In the context of hypersonic propulsion, shock reflection and detonation reflection are inevitable within the confined spaces of ODEs such as the inlet and combustor. Generally, there exist two distinct

[1] *State Key Laboratory of High Temperature Gas Dynamics, Institute of Mechanics, Chinese Academy of Sciences, No.15 Beisihuanxi Road, Beijing, China (100190), lihaoyang20@mails.ucas.ac.cn*
[2] *Department of Aeronautical and Aviation Engineering, The Hong Kong Polytechnic University, No.11 Yucai Road, Hung Hom, Kowloon, Hong Kong, China (999077), zijzhang@polyu.edu.hk*
[3] *State Key Laboratory of High Temperature Gas Dynamics, Institute of Mechanics, Chinese Academy of Sciences, No.15 Beisihuanxi Road, Beijing, China (100190), wangchun@imech.ac.cn*

configurations of steady shock reflection and detonation reflection: regular reflection (RR) and Mach reflection (MR) [2]. Nevertheless, as pointed out by Zhang et al. [3], once the MR is generated, it is very difficult to be stabilized in most cases. The destabilization is very unfavorable to the operation of an ODE because failure of the engine may occur. Therefore, when designing an ODE, the RR has more advantages, while the appearance of MR should be avoided as much as possible.

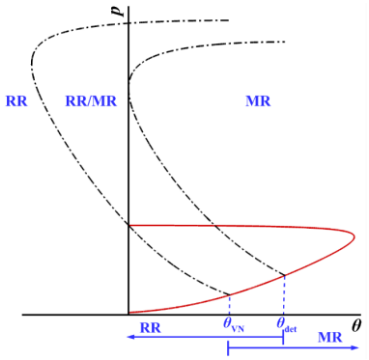

Fig 1. Diagram of typical pressure polars of shock reflection.

The shock wave is the basis of detonation. Firstly, von Neumann proposed a two-and-three shock model and two criteria that are known as the von Neumann (VN) criterion and the detachment criterion [4]. Classic shock polars obtained by solving the shock relations across an oblique shock wave (OSW) are used to simply illustrate the two criteria, as shown in Fig. 1. The VN criterion defines the minimum flow deflection angle, θ_{VN}, required for the theoretical existence of MR, while the detachment criterion gives the maximum flow deflection angle, θ_{det}, for RR. Above a specific flow Mach number, θ_{det} is greater than θ_{VN}. In this case, when the flow deflection angle falls between θ_{VN} and θ_{det}, both RR and MR are theoretically possible, implying a dual-solution domain.

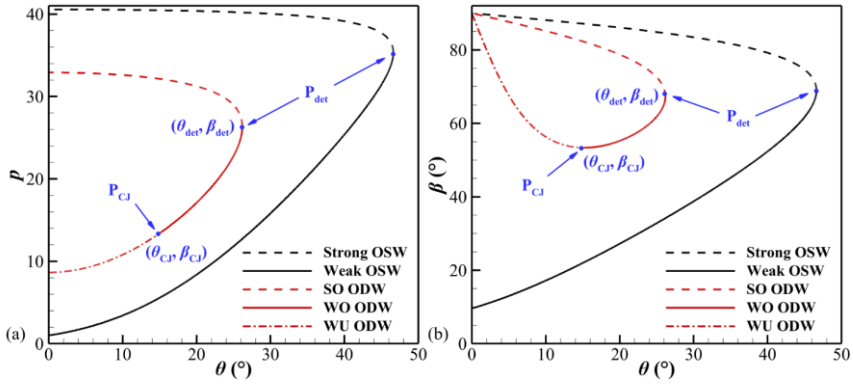

Fig 2. Diagram of typical shock and detonation polars.

However, a detonation wave differs from a shock wave fundamentally owing to the heat release from combustion. Typical shock and detonation polars showing the relationship between flow deflection angle θ and shock/detonation angle β are depicted in Fig. 2. The detachment point separates the shock polar into two segments: the weak solution (lower) and the strong solution (upper) of OSWs. The CJ point corresponding to the minimum detonation angle on the detonation polar represents the CJ condition of ODWs for a given Mach number. As a result, the detachment and CJ points separate the detonation polar into three segments: the strong overdriven (SO) detonation (upper), the weak overdriven (WO) detonation (middle), and the weak underdriven (WU) detonation (lower).

A stable ODW is necessary for the successful operations of ODEs. As pointed out by Pratt et al. [5], the flow deflection angle must lie within the range of $\theta_{CJ} < \theta < \theta_{det}$ for the stabilization of an ODW, i.e., the WO detonation. Therefore, most of the research about ODWs focuses on the part of WO detonation. While studies on WU detonation are relatively rare due to the opening discussion of its physical meaning. Many researchers [6,7] argued that the mathematical solution of WU detonation is non-existent physically. To date, the most prevailing opinion regarding the ODW solution for $\theta < \theta_{CJ}$ is that a CJ ODW is first formed and followed by a series of expansion waves. However, the point has not been verified further. Up to now, the correlation between pressure and deflection angle has not been

elucidated yet, even though it is crucial to the matching conditions of multiple waves in the detonation polar analysis of detonation reflection phenomena.

Motivated by the aforementioned unresolved issue, we expect to construct the relation between pressure p and deflection angle θ when $\theta < \theta_{CJ}$. Then, obtain a complete steady ODW reflection theory and its corresponding transition criteria. The proposed modellings of steady shock reflection with chemical heat release and the transition criteria hold immense potential in the design of ODE. By referring to the transition criteria, the occurrence of the MR phenomenon, which poses a significant challenge to ODEs, can be circumvented.

2. Physical and mathematical model

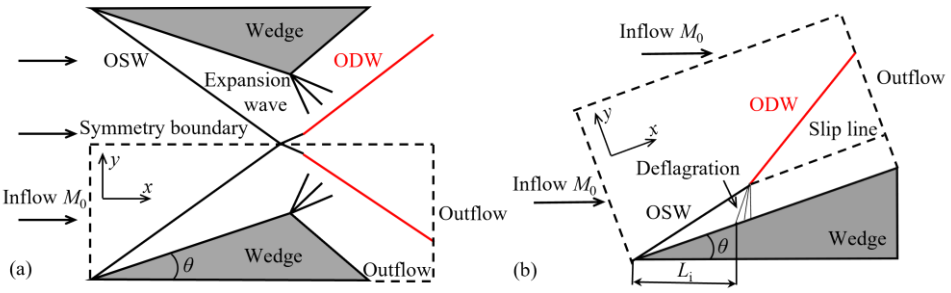

Fig 3. Schematic of double-wedge-induced oblique detonation (a) and single-wedge-induced oblique detonation (b).

To achieve the objectives of this study, two kinds of computational domains are adopted, as illustrated in Fig. 3. Specifically, Fig. 3(a) shows a novel symmetric double-wedge design of the ODE combustor. Two symmetric OSWs are first induced by the symmetric double wedges. Then, they interact with each other and form two symmetric ODWs. Figure 3(b) is employed to study the WU ODW structures with flow deflection angles of $\theta < \theta_{CJ}$. In this configuration, a typical ODW is induced by a two-dimensional, semi-infinite wedge. The computational domain is delineated by a dashed rectangular box.

The ODW flow field is modeled using the dimensionless reactive Euler equations. Combustion is modeled by a two-step chain-branching reaction model [8]. Based on the model, two kinds of submodels are employed. For the finite rate model, the induction zone length cannot be ignored, and is set to one certain value. For the quasi-equilibrium model, the lengths of the induction and chain termination zones are requested to be small enough. This study uses the non-oscillatory and non-free-parameter dissipation difference (NND) finite difference method [9] together with the Steger-Warming flux vector splitting method to solve the governing equations. To achieve sufficient resolution for the simulations, a third-order Runge–Kutta algorithm is chosen as the time-discretization scheme.

3. Results and discussion

3.1. Flow features of WU ODWs with $\theta < \theta_{CJ}$

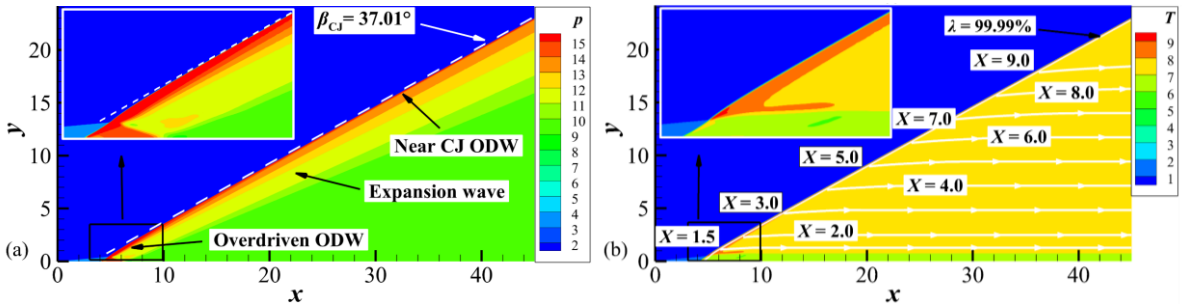

Fig 4. ODW pressure field (a) and temperature field (b) with induction zone length of L_i = 4 for the case: M_0 = 8 and θ = 8°.

The structure of an ODW with finite rate chemical reaction is first studied. As illustrated in Fig. 4, a single wedge initiates the ODW with induction zone length of L_i = 4. The inflow Mach number is set to be M_0 = 8 and the wedge angle θ = 8° that is less than the corresponding CJ angle (θ_{CJ} = 13.22°). The

initiation zone close to the ODW upstream exhibits an overdriven state, wherein its wave angle exceeds the CJ wave angle of β_{CJ} = 37.01° (the white dashed line in Fig. 4(a)). From Figs. 4(a) and 4(b), both the pressure and temperature behind overdriven ODW are considerably elevated. As the flow field develops downstream, the overdriven ODW gradually relaxes to be near CJ condition with the wave angle found to be consistent with the theoretical value. From pressure field shown in Fig. 4(a), a series of expansion waves arise following the ODW as mentioned in the previous studies [10,11]. To have a further insight into the flow structure of the ODW with expansion waves, streamlines originating at the end of the reaction zone, i.e., the location of the chain-recombination reaction progress variable $\lambda \approx 1$, are extracted. Herein, the non-dimensional length X is defined as $X = x/L_i$, where x denotes the initial position of streamlines.

The traditional detonation polars corresponding to the case in Fig. 4 are shown in Fig. 5 in red and black lines, together with the data along the streamlines. Specifically, the red solid line corresponds to the theory of SO and WO ODW, while the black solid line corresponds to the theory of WU ODW. These theories have been expounded upon in predecessors' study [12]. Points of different colors correspond to p-θ relationship on different streamlines. The initial pressure of the streamline of X = 1.5 surpasses the CJ pressure due to the overdriven nature of ODW close to its initiation point. As L increases, implying the streamline is getting far from the initiation point of ODW, and the effects of detonation initiation on the ODW surface are weaker and weaker. The initial pressure of streamline decreases gradually and tends towards the CJ pressure. Besides, the data of streamlines deviates from the theoretical solution of WU ODW. From Fig. 5(b), the points represent the β-θ relationship of the initial position of streamlines. The wave angle β also decreases and tends to CJ wave angle as the increase of X, which agrees with the observations from Fig .4.

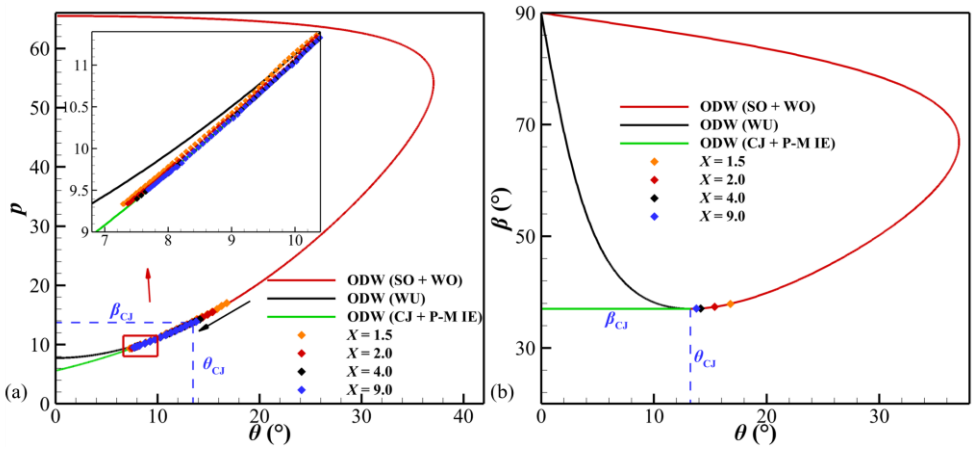

Fig 5. ODW pressure polar (a) and wave angle polar (b) for the case: M_0 = 8 and θ = 8°.

To solve the poor applicability of WU ODW theory, our study introduces a new addition represented by the green solid line, as shown in Fig. 5. According to the fact that the expansion wave will form behind CJ ODW when $\theta < \theta_{CJ}$, and that the expansion wave is isentropic in steady flow [13], we introduce the P-M IE theory to compare it with the WU ODW theory. The functions of the P-M IE theory shall be described in detail in section 3.3. From Fig. 5(a), the p-θ relation of streamlines is in line with the P-M IE theory. Additionally, the p-θ relation of the streamline closest to the downstream (i.e., X = 9.0) fits best with the P-M IE theory. This is because that the further downstream, the less affected the ODW is by the induction zone structure. The ODW will tend to CJ state and the expansion waves behind it can be approximately regard as P-M IE waves. Hence, what would be the flow field structure if the ODW fully develops and the induction zone is small enough until it can be neglected? This inquiry prompted us to study the ODW under the condition depicted in Fig. 4, where the chemical reaction rate is fast enough, that is the quasi-equilibrium chemical reaction model is adopted.

Figure 6 shows an ODW with the quasi-equilibrium chemical reaction model in the case where $\theta < \theta_{CJ}$. Compared to the flow field structure illustrated in Fig. 4, the ODW appears to have a simpler configuration. Similar to the ODW with an induction zone, the primary structure consists of a CJ ODW followed by a sequence of expansion waves. Nevertheless, there are conspicuous differences between ODWs with and without an induction zone. Notably, the flow field for the latter is more lucid and lacks interference from weaker waves. Additionally, a series of expansion waves radiate out from the leading-

edge point of the wedge. This key feature combined with the steady flow, characterizes this type of wave as a P-M IE wave. Based on the above results, we conclude that the P-M IE theory can be well applied to the whole zone behind the CJ ODW with a quasi-equilibrium chemical reaction model. Combining the CJ characteristic of wave surface, we call the theory CJ + P-M IE theory.

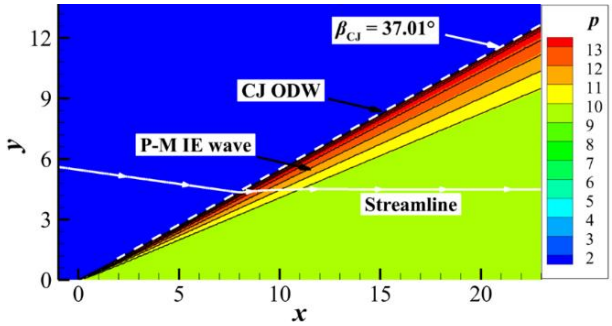

Fig 6. Pressure field of ODW without induction zone for the case: M_0 = 8 and θ = 8°.

To further validate the reliability of the P-M IE theory, we select a range of wedge angles from 2 to 13° to generate an ODW at an inflow Mach number M_0 = 6. The results obtained from the numerical simulation are then plotted in the form of an ODW polar, as illustrated in Fig. 7. The pressure obtained from the numerical results is derived from the region after the expansion wave, where the streamline is parallel to the wedge. As shown in Figs. 7(a) and (b), the numerical results for the pressure and wave angle are in good agreement with the solutions of CJ + P-M IE theory, indicating the accuracy of the theory. Taken together, these results suggest that the CJ + P-M IE theory is applicable to a CJ ODW following a series of expansion waves. Therefore, a new ODW polar will be utilized in the subsequent discussion, as shown in red line and green line in Fig. 7.

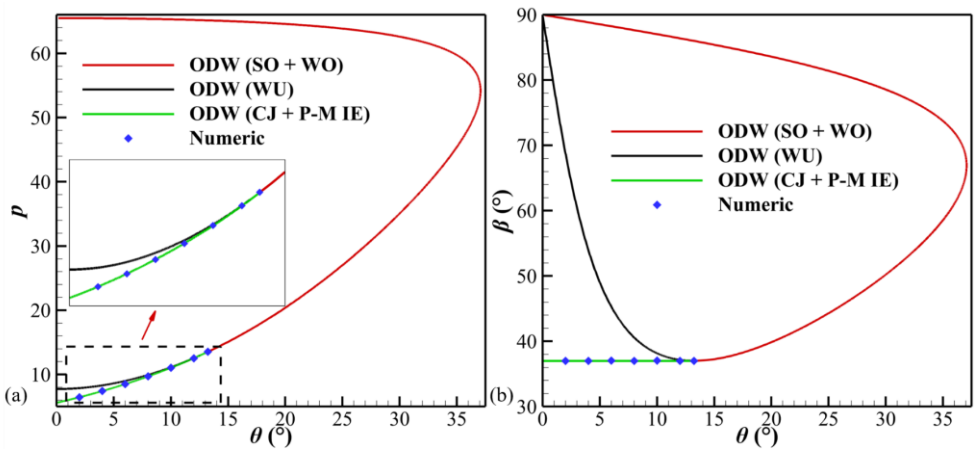

Fig 7. ODW pressure polar (a) and wave angle polar (b) for the case: M_0 = 8.

3.2. CJ + P-M IE in the matching relationship of pressure and flow deflection angle

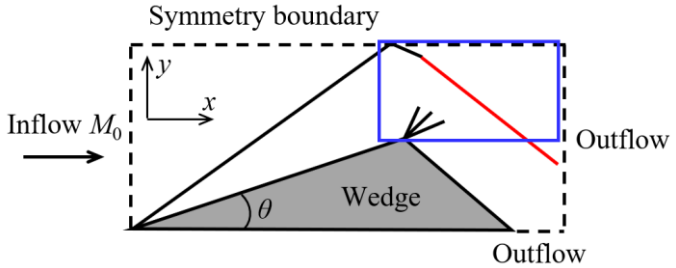

Fig 8. Schematic of shock-detonation reflection.

To verify the accuracy of shock-detonation wave reflection theory, our first step involves computation of stable RR and MR configurations under the same parameters in the dual solution domain. In the following cases, locally amplified flow fields are adopted to distinctly show the key characteristics of RR and MR, as shown in Fig. 8.

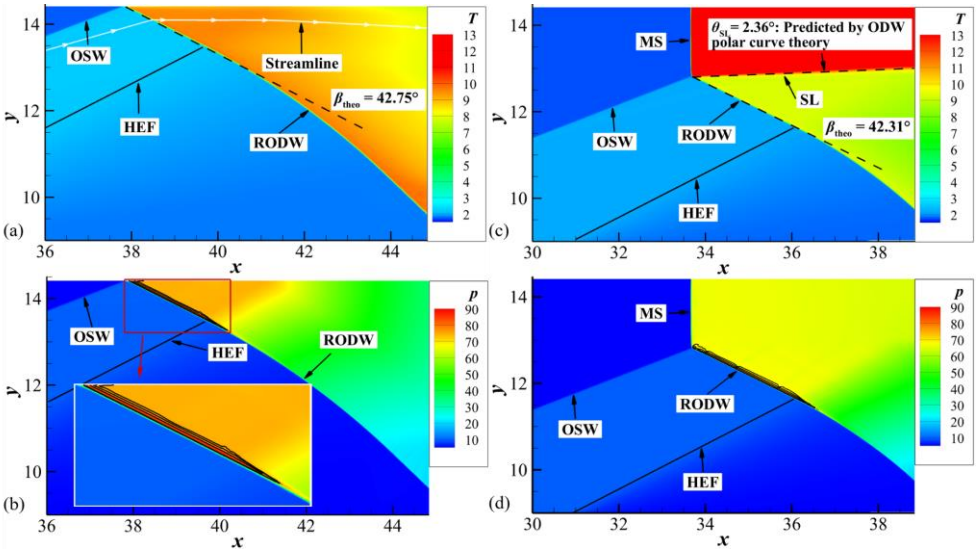

Fig 9. Temperature contours of RR (a) and MR (c) and pressure contours of RR (b) and MR (d) for the case: M_0 = 8 and θ = 16°. Black solid lines: pressure isoline.

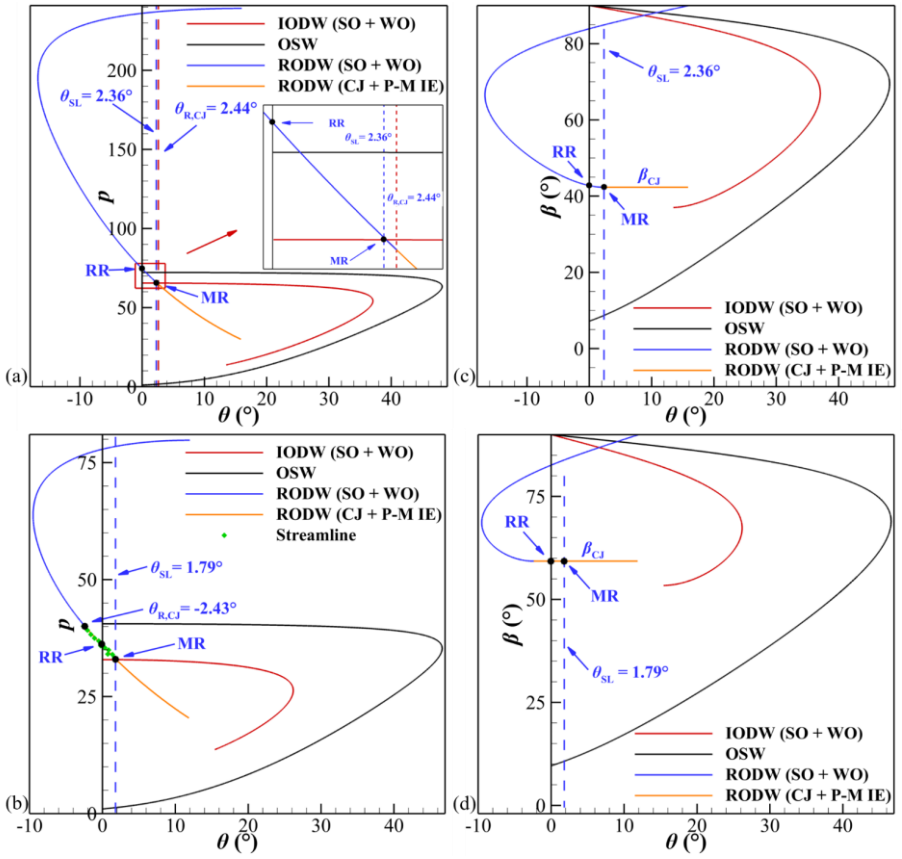

Fig 10. Illustration of the pressure shock-detonation polars for M_0 = 8, θ = 16° (a) and M_0 = 6, θ= 12°(b); wave angle shock-detonation polars for M_0 = 8, θ = 16°(c) and M_0 = 6, θ = 12°(d).

Under the conditions of M_0 = 8 and θ = 16°, the steady MR and RR structures are obtained using quasi-equilibrium model, which implies nearly equilibrium solutions, as shown in Fig. 9. The RR structure comprises an incident OSW and a reflected oblique detonation wave (RODW), as illustrated in Figs. 9(a) and (b). At the inflection point of the wedge, an expansion fan is formed, with the head of the expansion fan (HEF) labeled in the figures. The MR structure is more complicated than the RR structure. It also includes a Mach stem (MS) and a slip line (SL). There are two noteworthy characteristics of RR and MR. Firstly, the flow deflection angle behind RODW is crucial. For RR, the streamline runs parallel to the upper boundary, consistent with the accepted theory. For MR, it corresponds to the angle of the slip

line, which reflects the matching degree between post-RODW and post-MS flows. Figs 10(a) and (c) demonstrate that the theoretical angle of the slip line is 2.36°, which agrees well with the numerical result, depicted in a black dotted line in Fig. 9(c). Secondly, the angle of RODW is also significant. As shown in Fig. 10(c), the theoretical wave angles for RR and MR are slightly different. From the numerical results of Figs. 9(a) and (c), it can be deduced that both RODWs in RR and MR are basically consistent with the theoretical wave angle indicated by the black dotted lines. Besides, from Fig. 10(a), both RR and MR solutions in Fig .9 are located within the part of overdriven ODW (i.e., the segment of SO + WO RODW). The pressure isolines behind RODW are nearly parallel to the RODW, as shown in Figs. 9(b) and (d). Additionally, the streamline behind RODW is initially parallel to the upper boundary, but it gradually bends downstream owing to the impact of an expansion fan at the wedge inflection point, as shown in Fig. 9(a). It also leads to a downward bending of the RODW beyond the theoretical value of wave angle. This indicates that expansion waves (EWs) will cause the numerical results to deviate from the theoretical prediction.

Figure 11 shows the steady RR and MR structures are obtained based on the equilibrium hypothesis under the conditions of M_0 = 6 and θ = 12°. Unlike the case in Fig. 12, both RR and MR solutions in Fig .11 are located within the part of P-M IE ODW. This observation is supported by Figs. 10(b) and (d), which correspond to the conditions in Fig. 11. Although the structures of RR and MR in Fig. 11 bear resemblance to those in Fig. 9, it must be noted that the RODW is followed by a series of EWs, as shown in Figs. 11(b) and (d). The EWs in RR and MR are similar to that shown in Fig. 6 and originate from one point. However, the EW in RR has weaker expansion degree than that of the MR structure. The expansion angle of RR is merely the value of $-\theta_{R,CJ}$, while that of MR is the value of $\theta_{SL}-\theta_{R,CJ}$, as shown in Fig. 10(b). Besides, slip line angle and wave angles of RODW in RR and MR are consistent with the theoretical value indicated by the black dotted line, as shown in Figs. 11(a) and (c). The data of streamline crossing EW is extracted and displayed in Fig. 10(b). Obviously, the pressure of the streamline follows the CJ + P-M IE ODW theory well. Those characteristics provide numerical evidence for theoretical results.

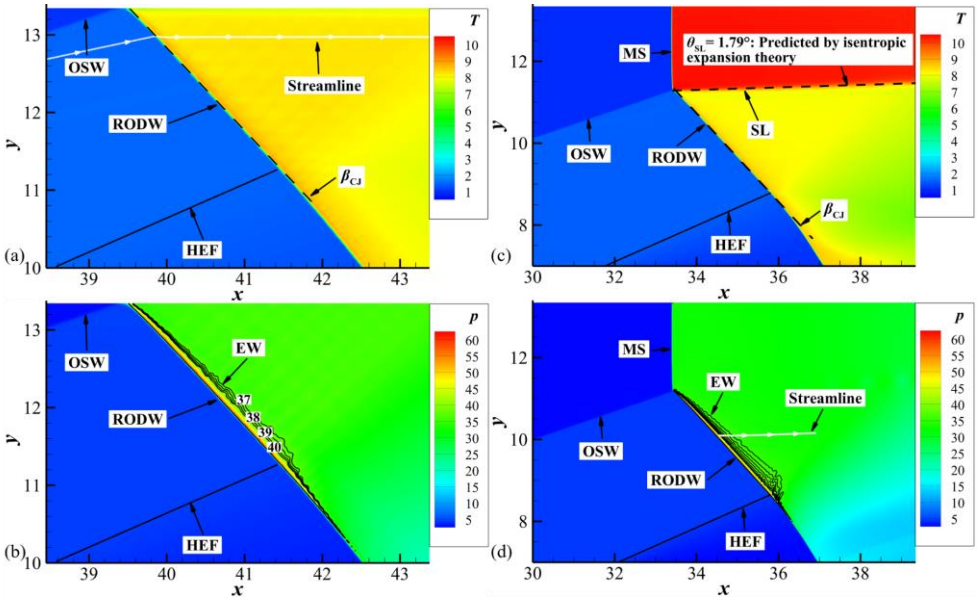

Fig 11. Temperature contours of RR (a) and MR (c) and pressure contours of RR (b) and MR (d) for the case: M_0 = 6 and θ = 12°. Black solid lines: pressure isolines.

The present study shows the RR and MR structures of numerical simulation, whereby crucial features such as the angles of the slip line and RODW are meticulously measured and compared against their corresponding theoretical values. The results demonstrate a remarkable degree of conformity between the obtained numerical data and the expected theoretical values. This agreement buttresses the reliability and accuracy of both the IE ODW theory and WO ODW theory.

3.3. Theory of steady shock-incident/detonation-reflection

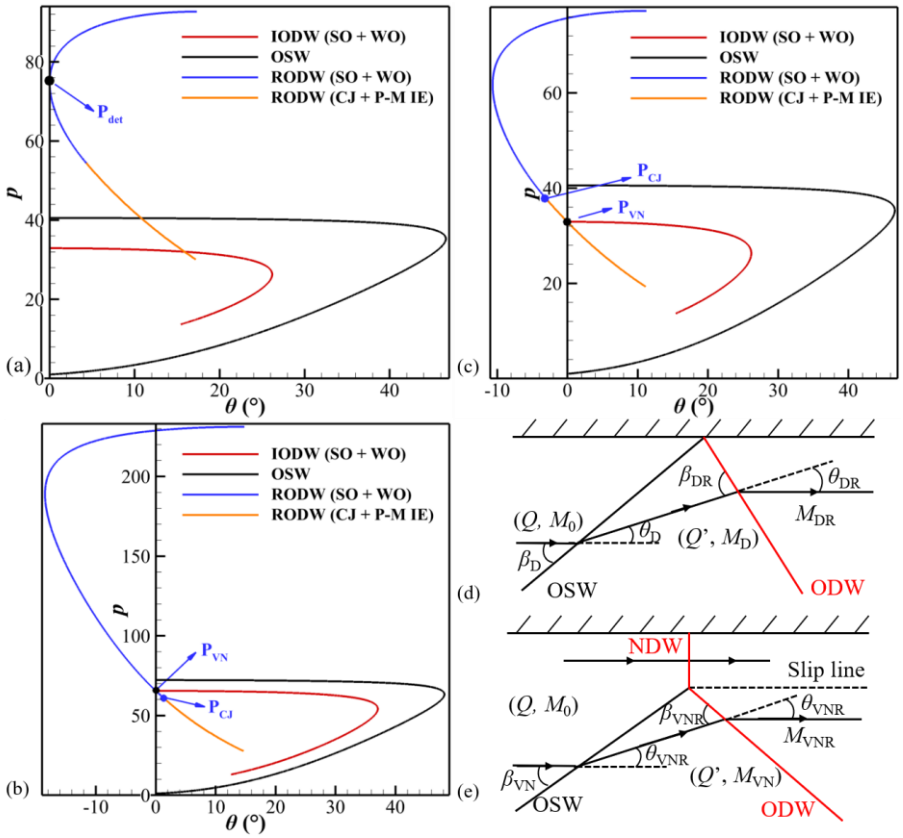

Fig 12. Illustration of the shock-detonation reflection criteria: detonation polar corresponding to the detachment criterion (a), VN criterion in part of SO + WO ODW (b), VN criterion in part of CJ + P-M IE ODW (c), diagram of RR (d), and diagram of MR (e).

The shock-detonation reflection theory is established in our study based on the model shown in Fig. 3(a). Besides, the chemical reaction zone including induction length and heat release length is enough short, with heat rapidly released, that is, an equilibrium hypothesis is adopted. Based on the above assumptions, we first formulate the detachment criterion. As shown in Fig. 12(a), it is illustrated by shock and detonation polar lines, which contain four segments. Specifically, the blue line represents the part of reflected WO ODW, while the orange line denotes the part of reflected ODW followed by the P-M IE wave. The black line is polar of the incident shock wave, while the red line represents the detonation polar corresponding to the initial flow conditions. According to the case that the reflected detonation polar line is tangent to the y-axis at the detachment point, as shown in Fig. 12(a), the detachment criterion θ_D can be obtained from the following equations.

First, the relationship between the Mach number before and after the OSW can be expressed as follows:

$$M_D^2 \sin^2(\beta_D - \theta_D) = S_M(M_0, \beta_D), \tag{1}$$

$$S_M(M, \beta) = \frac{2 + (\gamma - 1)M^2 \sin^2 \beta}{2\gamma M^2 \sin^2 \beta - \gamma + 1}, \tag{2}$$

where β_D is the incident shock angle and M_D is the Mach number behind the incident shock, as shown in Fig. 12(d). They both correspond to the detached state.

Then, according to the relationship between OSW angle and deflection angle, we can obtain the equation:

$$\tan\theta_D = S_\theta(M_0, \beta_D), \tag{3}$$

$$S_\theta(M, \beta) = \frac{2M^2 \sin^2 \beta - 2}{[2 + M^2(\gamma + 1 - 2\sin^2 \beta)]\tan\beta}, \tag{4}$$

Next, according to the define of detachment criterion, the deflection angle θ_D of the incident OSW should be equal to that of the reflected ODW. Thus, their tangent values should also be equal. The equations are as follows:

$$S_\theta(M_0, \beta_D) = D_\theta(Q'(M_0, \beta_D), M_D, \beta_{DR}), \tag{5}$$

$$D_\theta(Q, M, \beta) = \frac{M^2 \sin^2\beta - 1 + \sqrt{(M^2 \sin^2\beta - 1)^2 - 2Q(\gamma^2 - 1)M^2 \sin^2\beta}}{\tan\beta(\gamma M^2 \sin^2\beta + 1 - \sqrt{(M^2 \sin^2\beta - 1)^2 - 2Q(\gamma^2 - 1)M^2 \sin^2\beta}) + \frac{\gamma + 1}{2} M^2 \sin 2\beta}, \tag{6}$$

where the $D_\theta(Q, M, \beta)$ is the tangent value of ODW deflection angle and its derivation is shown in Appendix. $Q'(M_0, \beta_D)$ denotes the nondimensionalized chemical heat release before reflected detonation, which can be obtained by dividing the nondimensionalized chemical heat release Q by the temperature ratio after OSW to before OSW $S_T(M_0, \beta_D)$, as shown in Eqs. (7) and (8). β_{DR} is a critical detonation wave angle for the attached detonation, which corresponds to the maximal value of deflection angle θ_{DR}. Thus, to determine β_{DR}, we set the first derivative of the ODW deflection angle tangent function to zero, as shown in Eq. (9). The detail expression of Eq. (9) is shown in Appendix. Combining Eq. (1)-(9), the θ_D can be derived.

$$Q'(M, \beta) = \frac{Q}{S_T(M, \beta)}, \tag{7}$$

$$S_T(M, \beta) = \frac{[2\gamma M^2 \sin^2\beta - (\gamma - 1)][(\gamma - 1)M^2 \sin^2\beta + 2]}{(\gamma + 1)^2 M^2 \sin^2\beta}, \tag{8}$$

$$\frac{\partial D_\theta}{\partial \beta}(Q'(M_0, \beta_D), M_D, \beta_{DR}) = 0, \tag{9}$$

If the reflected detonation polar and incident detonation polar intersect at the VN point, it can be deduced that the flow deflection angle conforms to the VN criterion, denoted as θ_{VN}. For VN criterion, the key is the pressure matching on both sides of the slip line, as shown in Fig .12(e). One side is the pressure behind the Mach stem, that is the normal detonation wave. The other side is the pressure behind the reflected ODW. However, this differs from previous research conducted by Xue et al. [14], which exclusively examined shock reflection. With regards to shock-detonation reflection, two cases should be considered. Specifically, if the flow deflection angle of reflected detonation θ_{VNR}, exceeds the CJ deflection angle θ_{CJR}, such that the VN point resides on the section of WO ODW, as shown in Fig. 12(b), then Eq. (10) is satisfied. Conversely, when the flow deflection angle of reflected detonation θ_{VNR} falls below the CJ deflection angle θ_{CJR}, such that the VN point lies on the part of IE ODW, as shown in Fig. 12(c), then Eq. (11) holds true. The two kinds of pressure balance equations are expressed as follows:

$$D_p(Q, M_0, \frac{\pi}{2}) = S_p(M_0, \beta_{VN}) D_p(Q'(M_0, \beta_{VN}), M_{VN}, \beta_{VNR}), \quad \theta_{VNR} > \theta_{CJR}, \tag{10}$$

$$D_p(Q, M_0, \frac{\pi}{2}) = S_p(M_0, \beta_{VN}) E_p(M_{VNR}), \quad \theta_{VNR} < \theta_{CJR}, \tag{11}$$

where β_{VN} is the incident detonation wave angle, M_{VN} is the Mach number behind the incident detonation wave, and β_{VNR} is the reflected detonation wave angle, as shown in Fig. 12(e). They all correspond to the state of VN criterion. Besides, the $S_P(M, \beta)$ represents the pressure ratio after OSW to before OSW. While $D_P(Q, M, \beta)$ and $E_P(M)$ represent the pressure ratio after reflected ODW to before reflected ODW. Their expressions are as follows. The derivation of $S_P(M, \beta)$ is simple and will not be showed here. $E_P(M)$ can be derived from isentropic relation along streamline. While the derivations of $D_P(Q, M, \beta)$ is showed in Appendix in detail.

$$S_p(M, \beta) = 1 + \frac{2\gamma}{\gamma + 1}(M^2 \sin^2\beta - 1), \tag{12}$$

$$D_p(Q, M, \beta) = 1 + \frac{\gamma}{\gamma + 1}(M^2 \sin^2\beta - 1 + \sqrt{(M^2 \sin^2\beta - 1)^2 - 2Q(\gamma^2 - 1)M^2 \sin^2\beta}), \tag{13}$$

$$E_p(M) = p_{CJR}\left(\frac{1+\frac{\gamma-1}{2}M_{CJR}^2}{1+\frac{\gamma-1}{2}M^2}\right)^{\frac{\gamma}{\gamma-1}}, \tag{14}$$

where the p_{CJR} and M_{CJR} represent the pressure ratio after ODW to before ODW and Mach number of post reflected ODW corresponding to the CJ state, respectively. They can be expressed by the following functions:

$$p_{CJR} = D_p(Q'(M_0, \beta_{VN}), M_{VN}, \beta_{CJR}), \tag{15}$$

$$M_{CJR} = \frac{M_{VN}\sin\beta_{CJR}}{\sqrt{p_{CJR}\rho_{CJR}}\sin(\beta_{CJR}-\theta_{CJR})}, \tag{16}$$

where the β_{CJR} and θ_{CJR} are the reflected detonation wave angle and flow deflection angle under CJ state, respectively. The ρ_{CJR} represents the density ratio after ODW to before ODW. The detail derivation about Eq. (16) is shown in Appendix. The β_{CJR}, θ_{CJR} and ρ_{CJR} can be obtained by following functions:

$$\beta_{CJR} = \sin^{-1}\left(\frac{M_{CJ}(Q'(M_0, \beta_{VN}))}{M_{VN}}\right), \tag{17}$$

$$M_{CJ}(Q) = \sqrt{[1+(\gamma^2-1)Q]+\sqrt{[1+(\gamma^2-1)Q]^2-1}}, \tag{18}$$

$$\tan\theta_{CJR} = D_\theta(Q'(M_0, \beta_{VN}), M_{VN}, \beta_{CJR}), \tag{19}$$

$$\rho_{CJR} = \frac{\tan\beta_{CJR}}{\tan(\beta_{CJR}-\theta_{CJR})}, \tag{20}$$

In addition to meeting the conditions for pressure matching, it is also necessary to meet two other conditions need. One is the relationship between the Mach number before and after the incident OSW, as shown in Eq. (21). The other is that the flow deflection angle of the incident OSW is equal to that of the reflected ODW, as shown in Eq. (31)-(33).

$$M_{VN}^2\sin^2(\beta_{VN}-\theta_{VN}) = S_M(M_0, \beta_{VN}), \tag{21}$$

$$\tan\theta_{VN} = S_\theta(M_0, \beta_{VN}), \tag{22}$$

$$\tan\theta_{VNR} = D_\theta(Q'(M_0, \beta_{VN}), M_{VN}, \beta_{VNR}), \tag{23}$$

$$S_\theta(M_0, \beta_{VN}) = D_\theta(Q'(M_0, \beta_{VN}), M_{VN}, \beta_{VNR}), \tag{24}$$

For the case of $\theta_{VNR} > \theta_{CJR}$, there are five main variables: β_{VN}, M_{VN}, θ_{VN}, β_{VNR}, and θ_{VNR}. Therefore, combining Eqs. (19) and (22)-(24), all variables can be solved. However, for the case of $\theta_{VNR} < \theta_{CJR}$, an additional variable M_{VNR} is introduced. Thus, a Prandtl-Meyer flow relationship is added, as shown in Eq. (25). Combining Eq. (11) and (21)-(25), β_{VN}, M_{VN}, θ_{VN}, β_{VNR}, θ_{VNR} and M_{VNR} can be solved.

$$\Delta\theta = \theta_{VNR} - \theta_{CJR} = \theta(M_{VNR}) - \theta(M_{CJR}), \tag{25}$$

$$\theta(M) = \sqrt{\frac{\gamma+1}{\gamma-1}}\arctan\sqrt{\frac{\gamma-1}{\gamma+1}(M^2-1)} - \arctan\sqrt{M^2-1}, \tag{26}$$

So far, the detachment and VN criteria of shock-detonation reflection can be obtained.

3.4. The verification of shock-detonation transition criteria

With the detachment criterion and VN criterion of shock-detonation transition solved theoretically above, a numerical investigation is performed in this section to validate the theories. A simple method is used to identify the critical transition angles in shock-detonation reflection, which is also employed by Peng et al [15]. This method involves initiating calculations at one wedge angle, and acquiring a steady flow field of RR. Then, the wedge angle is incremented by 0.1° and the calculation is repeated until convergence is reached again. Throughout the alteration of the wedge angle, the length of the wedge and the height of the flow channel (i.e., the height from the inflection point of the wedge to the upper boundary) remain fixed. This process is iterated until a MR configuration eventually emerges, thereby yielding the detachment angle. Subsequently, decreasing the angle enables us to determine the von Neumann angle.

The cases of different M_0 are calculated and the results are summarized in Fig. 13. The black solid line represents the detachment criterion. The red solid line is the VN criterion in accordance with the WO ODW theory, while the red dotted line is associated with the P-M IE theory. The blue circles and diamonds indicate numerical simulation results of detachment angles and VN angles, respectively. From Fig. 13, we can find numerical results are coincident with the theoretical ones. The computations can confirm that the shock-detonation reflection theory and transition criteria are accurate in our study.

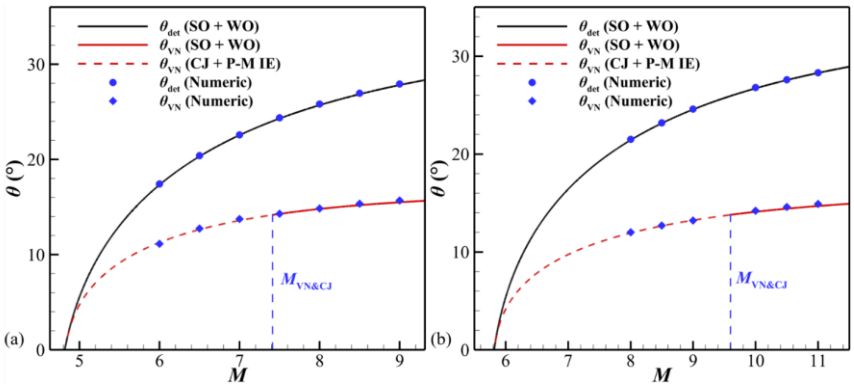

Fig 13. The shock-detonation reflection transition criteria of theory and numerical simulation under different Q: Q = 20 (a); Q = 30 (b).

4. Conclusions

The field of shock reflection theory has been the subject of extensive investigation. Conversely, the study of detonation reflection theory is notably scarce. Thus, our current research endeavors to establish a new shock-detonation reflection theory and elucidate its transition criteria. This novel theory has not been previously explored and holds promise for application in innovative ODE designs.

Initially, we utilized the reactive Euler equations, coupled with a two-step induction-reaction kinetic model, to simulate ODWs in instances where the deflection angle $\theta < \theta_{CJ}$. A CJ ODW emerges, which is followed by a sequence of expansion waves. The result contradicts the classical solution of WU ODW theory. If the length of the induction zone is zero, it is possible to view the expansion waves as P-M expansion waves. Based on our findings, we hereby introduce a P-M IE theory, aimed at re-establishing the correlation between pressure and deflection angle for the section of WU detonation polar. Finally, detachment and VN criteria were confirmed under two different Q values. The numerical results exhibit near-consistency with the theoretical predictions. These numerous verifications and small discrepancies exemplify the reliability and accuracy of the proposed theory in this study.

Appendix

The relationship between detonation wave angle and flow deflection angle has been given by Yang et al. [16], as shown in Eq. (A1).

$$\frac{\tan\beta}{\tan(\beta-\theta)}=\frac{(\gamma+1)M^2\sin^2\beta}{\gamma M^2\sin^2\beta+1-\sqrt{(M^2\sin^2\beta-1)^2-2Q(\gamma^2-1)M^2\sin^2\beta}}, \tag{A1}$$

Combining the trigonometric function relation Eq. (A2), the tangent value of ODW deflection angle $D_\theta(Q, M, \beta)$ can be obtained, as shown in Eq. (6).

$$\tan(\beta-\theta)=\frac{\tan\beta-\tan\theta}{1+\tan\beta\tan\theta}, \tag{A2}$$

The first derivative of the ODW deflection angle tangent function Eq. (9) is as follow:

$$\frac{\partial D_\theta}{\partial\beta}(Q,M,\beta)=\frac{(M^2\sin 2\beta+temp1)temp3-(M^2\sin^2\beta-1+temp0)temp4}{(temp3)^2}, \tag{A3}$$

$$\begin{cases} temp0(Q,M,\beta)=\sqrt{(M^2\sin^2\beta-1)^2-2Q(\gamma^2-1)M^2\sin^2\beta}, \\ temp1(Q,M,\beta)=\dfrac{(M^2\sin^2\beta-1)M^2\sin 2\beta-Q(\gamma^2-1)M^2\sin 2\beta}{temp0}, \\ temp2(Q,M,\beta)=\tan\beta(\gamma M^2\sin^2\beta+1-temp0), \\ temp3(Q,M,\beta)=temp2+(\gamma+1)M^2\dfrac{\sin 2\beta}{2}, \\ temp4(Q,M,\beta)=\dfrac{temp2}{\tan\beta\cos^2\beta}+\tan\beta(\gamma M^2\sin 2\beta-temp1)+(\gamma+1)M^2\cos 2\beta, \end{cases} \tag{A4}$$

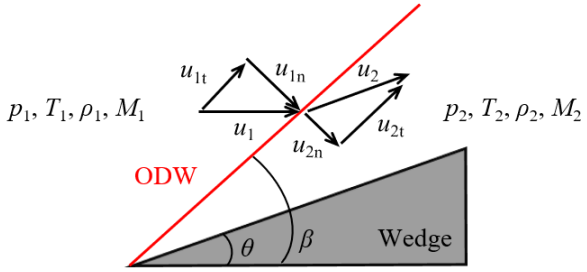

Fig 14. Diagram of an ideal ODW.

The derivations of $D_p(Q, M, \beta)$ and $E_p(M)$ are as follow. According to the equation of continuity Eq. (A5) and momentum conservation equation Eq. (A6), the pressure ratio after and before ODW can be solved, as shown in Eq. (A7).

$$\rho_1 u_{1n}=\rho_2 u_{2n}, \tag{A5}$$

$$p_1+\rho_1 u_{1n}^2=p_2+\rho_2 u_{2n}^2, \tag{A6}$$

$$\frac{p_2}{p_1}=1+(1-\frac{\rho_1}{\rho_2})\cdot\frac{\rho_1}{\rho_2}\cdot u_{1n}^2=1+(1-\frac{\rho_1}{\rho_2})\cdot\frac{\gamma}{\gamma RT_1}\cdot u_1^2\sin^2\beta=1+(1-\frac{\rho_1}{\rho_2})\gamma M_1^2\sin^2\beta, \tag{A7}$$

From Fig. 14, the Eqs. (A8) and (A9) can be obtained easily. Then, based on the fact that $u_{1t}= u_{2t}$, the Eq. (A10) can be obtained combining with the Eq. (A5),

$$\tan\beta=\frac{u_{1n}}{u_{1t}}, \tag{A8}$$

$$\tan(\beta-\theta)=\frac{u_{2n}}{u_{2t}}, \tag{A9}$$

$$\frac{\rho_2}{\rho_1}=\frac{u_{1n}}{u_{2n}}=\frac{\tan\beta}{\tan(\beta-\theta)}=\frac{(\gamma+1)M^2\sin^2\beta}{\gamma M^2\sin^2\beta+1-\sqrt{(M^2\sin^2\beta-1)^2-2Q(\gamma^2-1)M^2\sin^2\beta)}}, \tag{A10}$$

Combining Eqs. (A7) and (A10), the Eq. (13) can be obtained.

The relation of Mach number after and before ODW is shown as Eq. (A11). Substituting the corresponding parameters into the Eq. (A11), as shown in Eq. (A12), the Eq. (16) can be obtained.

$$\frac{M_2^2\sin^2(\beta-\theta)}{M_1^2\sin^2\beta}=(\frac{u_{2n}}{u_{1n}})^2(\frac{c_1}{c_2})^2=(\frac{\rho_1}{\rho_2})^2(\frac{T_1}{T_2})=\frac{\rho_1}{\rho_2}\cdot\frac{p_1}{p_2}, \tag{A11}$$

$$\frac{M_{CJR}^2\sin^2(\beta_{CJR}-\theta_{CJR})}{M_{VN}^2\sin^2\beta_{CJR}}=\frac{1}{p_{CJR}\rho_{CJR}}. \tag{A12}$$

References

1. Wolański, P.: Detonative propulsion. Proc. Combust. Inst. (2013).
2. Hornung, H.: Regular and Mach reflection of shock waves. Annu. Rev. Fluid Mech. (1986).

3. Zhang, Z., Liu, Y., Wen, C.: Mechanisms of the destabilized Mach reflection of inviscid oblique detonation waves before an expansion corner. J. Fluid Mech. (2022).
4. Von Neumann, J.: Oblique Reflection of Shocks, Explosives Research. Technical Report 12, Bureau of Ordinance, Washington, USA, 1943.
5. Pratt, D. T., Humphrey, J. W., Glenn, D. E.: Morphology of Standing Oblique Detonation Waves. J. Propuls. Power (1991).
6. Buckmaster, J., Lee, C. J.: Flow Refraction by an Uncoupled Shock and Reaction Front. AIAA J. (1990).
7. Emanuel, G., Tuckness, D. G.: Steady, Oblique, Detonation Waves. Shock Waves (2004).
8. Ng, H. D., Radulescu, M. I., Higgins, A. J., Nikiforakis, N., Lee, J. H. S.: Numerical investigation of the instability for one-dimensional Chapman–Jouguet detonations with chain-branching kinetics. Combust. Theory Model. (2005).
9. Zhang, H. X.: Non-oscillatory and non-free-parameter dissipation difference scheme. Acta Mech. Sin. (1988).
10. Ashford, S. A., Emanuel, G.: Wave Angle for Oblique Detonation Waves. Shock Waves (1994).
11. Verreault, J. A., Higgins, J., Stowe, R. A.: Formation and structure of steady oblique and conical detonation waves. AIAA J. (2012).
12. Powers, J. M., Stewart, D. S.: Approximate solutions for oblique detonations in the hypersonic limit. AIAA J. (1992).
13. Fickett, W., Davis, W. C.: Detonation: Theory and Experiment (Courier Corporation, 2000).
14. Xue, L., Wang, C., Cheng, K.: A study on the RR-to-MR transition of shock wave reflections near the leading edge in hypersonic flows. J. Fluid Mech. (2021).
15. Peng, J., Zhang, Z., Hu, Z., Jiang, Z.: A theoretical and computational study of the vibration excitation on the transition criteria of shock wave reflections. Aerosp. Sci. Technol. (2019).
16. Yang, P., Li, H., Chen, Z., Wang, C., Teng, H.: Numerical investigation on movement of triple points on oblique detonation surfaces. Phys. Fluids (2022).